Room Temperature Synthesis of Highly Compact TiO₂ Coatings by Vacuum Kinetic Spraying to Serve as a Blocking Layer in Polymer Electrolyte-Based Dye-Sensitized Solar Cells

Jeeae Heo, P. Sudhagar, Hyungkwon Park, Woohyung Cho, Yong Soo Kang, and Changhee Lee

Vacuum kinetic spraying (VKS) was used to form a blocking layer (BL) in order to increase the efficiency of dye-sensitized solar cells. Nano-sized TiO₂ powders were deposited on fluorine-doped tin oxide (FTO) glass while varying the coating parameters including the mass flow, substrate transverse speed, and number of coating passes in order to control the thickness of the BL. Compared to the cell without a BL, the open-circuit voltage and short-circuit current density of the solar cell with a VKS-coated BL were noticeably improved. Consequently, the photoconversion efficiency increased up to 5.6%, which is significantly higher than that of a spin-coated BL.

1. Introduction

Photovoltaic systems have recently become more promising spurring a number of research groups to develop novel excitonic solar cells. In this context, dye-sensitized solar cells (DSSCs) have received a great deal of attention as an alternative to conventional silicon photovoltaic cells due to their low cost, color, and possibility for use in a variety of applications (Ref 1). A DSSC is composed of a dye-sensitized semiconducting oxide film (TiO₂, ZnO, and SnO₂) deposited on a transparent conductive oxide substrate (TCO) that serves as the working electrode (i.e., the so-called photoanode). A Pt-coated TCO substrate sealed with a dye-sensitized photoanode with a face-to-face configuration acts as the counter electrode. The space between these two electrodes is filled with an electrolyte that plays the role of a conducting mediator (Ref 2). A broad range of DSSC architectures has been established for liquid-type DSSCs using different types of photoanodes (Ref 3, 4), redox mediators (Ref 5), dye sensitizers (Ref 6), electrolytes (Ref 7), catalytic counter electrodes (Ref 8), and co-adsorbants (Ref 9), demonstrating efficiencies of up to 12.3% (Ref 10). Replacing the liquid electrolyte with a solid electrolyte (Ref 11) or quasi-solid electrolyte (Ref 12) would help overcome most issues concerning fabrication (electrolyte leakage) and the product lifetime.

One of the major issues encountered in DSSCs is electron recombination at the TiO₂/TCO interface (Ref 13, 14). The uncovered sites of mesoporous TiO₂ particles at the TCO layer can create recombination pathways that allow the electrons to pass from the TCO layer to the electrolyte. Further, these revisiting electrons can recombine with the hole-transport medium and greatly decrease the current output of the solar cell. Applying a blocking layer (BL) between the mesoporous TiO₂ layer (mp-TiO₂) and TCO substrate prevents direct physical contact between the electrolyte and TCO layer and increases the efficiency of DSSCs (Ref 15-17). In addition, it provides more electron pathways from mp-TiO₂ to TCO because of the larger contact area and improved adherence of the interface (Ref 3).

Typically, the BL consists of a compact layer of TiO₂ with a thickness of about 20-100 nm. A wide range of techniques have been developed to deposit pore-free compact thin TiO₂ films, such as sputtering (Ref 18), spray pyrolysis (Ref 17), and liquid coating techniques including spin coating (Ref 19) and dip coating from titania precursors (Ref 20). Although a highly dense BL coating can be achieved by the sputtering technique, it requires an expensive source target and various coating parameters. In the spray pyrolysis technique, it is difficult to control the film thickness, and reproducibility is also challenging. For

Jeeae Heo, Hyungkwon Park, and **Changhee Lee**, Kinetic Spray Coating Laboratory, Division of Materials Science and Engineering, Hanyang University, Seoul 133-791, Republic of Korea; and **P. Sudhagar, Woohyung Cho,** and **Yong Soo Kang**, Department of Energy Engineering, Hanyang University, Seoul 133-791, Republic of Korea. Contact e-mail: chlee@hanyang.ac.kr.

these reasons, solution process-based coating techniques are often recommended, but the resulting diminished thickness is not sufficient to completely cover the TCO layer. Moreover, the performance of a DSSC can be reduced by increasing the series resistance due to the formation of voids and impurities (Ref 21-23). Considering charge injection from the mp-TiO$_2$ layer to TCO, a thicker and defected BL reduces the efficiency of the solar cell by hindering charge injection. Therefore, fabricating a BL with an optimum thickness and a crack-free layer is necessary to achieve a high current collection in the DSSC (Ref 24).

Vacuum kinetic spray (VKS) coating, i.e., the so-called aerosol deposition method (ADM), is a novel coating technique which offers a feasible way to tailor the thickness of compact films from a few nanometers to several microns at room temperature (Ref 25). The coating formation in the VKS process is related to the fragmentation and consolidation of submicron-sized ceramic particles upon impact (Ref 25-28). When aerosol particles impact the substrate with a high velocity, they are fractured and undergo plastic deformation (Ref 29). This creates a new surface with a high energy where strong bonding of particles occurs in order to decrease the surface energy (Ref 28). The aerosol particles are sprayed continuously, and a coating grows on top of the previously formed coating (Ref 30, 31). Compared to other methods, the VKS technique offers a more uniform and dense coating layer, and the process is quicker due to the fast deposition rate.

Based on previous findings, the VKS technique is proposed in order to achieve a uniform and dense TiO$_2$ BL in DSSCs. The blocking performance at the TCO/mp-TiO$_2$ interface was compared to those of a conventional spin-coated BL as well as a DSSC without a BL.

2. Experimental

2.1 Material Preparation and Vacuum Kinetic Sprayed TiO$_2$ BL Coating

Commercial TiO$_2$ powder (99.6% purity, Alfa Aesar, USA) and fluorine-doped tin oxide (FTO)-coated glass were used as the feedstock material and substrate, respectively. Prior to VKS deposition, the powder was pretreated by a jet-milling process in order to increase the strain and defect density, which is expected to improve the deposition efficiency (Ref 25, 32). In addition, the jet-milled powders were dried in an oven for around 1 h at 120 °C, and the FTO substrates were cleaned by ultrasound before the coating experiments.

A schematic illustration of the VKS equipment is presented in Fig. 1. The vibrated ceramic particles in the aerosol chamber were transported through a convergent-barrel-type slit nozzle with an orifice size of 5.0×0.4 mm^2 into the deposition chamber. The vacuum was generated by rotary and booster pumps. Helium was used as the carrier gas, and the pressure was fixed at 0.6 MPa by a gas regulator. The mass flow rate (MF) was controlled in the range of 3-9 L/min with an interval of 2 L/min, and the

traverse speed (T_s) was set to 1 or 5 mm/s. The number of passes (n) was fixed at 2. The coating parameters of the VKS process are shown in Table 1. A variety of TiO$_2$-coated electrodes with different coating thicknesses were prepared by varying the VKS parameters to investigate the BL performance by means of the DSSC assembly. In addition, a spin-coated TiO$_2$ film (Spin BL) was prepared using a Ti (IV) bis (ethyl acetonato)-diisopropoxide solution in 2 wt.% 1-butanol in order to compare the performance of VKS-coated BL layers with conventional BL coatings.

2.2 DSSC Assembly

The VKS-coated TiO$_2$ BL layers, (a) VKS1-BL, (b) VKS2-BL, and Spin BL were fabricated on FTO substrates and applied as a BL in DSSCs. After preparing the BL on FTO substrates, the mesoporous TiO$_2$ layer with a thickness of about 6 μm was prepared on the BL/FTO substrate using the as-received commercially available TiO$_2$ paste (18 NR-T, Dyesol). Then, a second layer with a thickness of approximately 5 μm was deposited using commercial 200-nm light-scattering TiO$_2$ particles (WER 2-O, Dyesol) by a doctor blade technique and subsequently sintered at
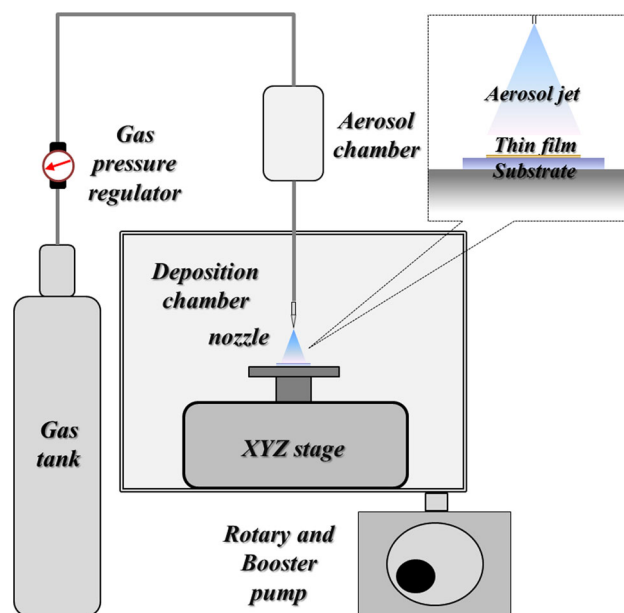

Fig. 1 Schematic image of the vacuum kinetic spray coating system

Table 1   Vacuum kinetic spraying parameters

Vacuum chamber pressure, torr	6.0×10^{-2}
Gas pressure, MPa	0.6
Nozzle type	Slit nozzle
Orifice size of nozzle, mm^2	5.0×0.4
Substrate traverse speed, mm s^{-1}	1, 5
He gas flow, L min^{-1}	3, 5, 7, 9
The number of passes	2
Distance from the nozzle to substrate, mm	8

450 °C for 30 min under an ambient atmosphere. Following heat treatment, the electrodes were immersed in a dye solution (0.5 mM cis-diisothiocyanato-bis (2,2'-bipyridyl-4,4'-dicarboxylato) ruthenium (II) bis(tetrabutylammonium), N719, Solaronix) in acetonitrile (ACN, Wako)/tert-butyl alcohol (t-BuOH, Wako) (1/1, v/v) and held at room temperature. The gel-type polymer electrolyte used in the DSSCs was prepared according to the following method. A blend of polyethylene oxide (PEO: $Mw = 1$ Mg/mol) and polyethylene glycol dimethyl ether (PEGDME: $Mw = 500$ g/mol) with a [-O-]:[KI]:[I$_2$] molar ratio of 10:1:0.1 was prepared and fixed at a ratio of 4:6 (w/w). The detailed electrolyte preparation procedure has been reported elsewhere (Ref 7). The oligomer-based electrolyte was applied on a dye-sensitized photoanode and dried at 80 °C for a few hours. Finally, Pt counter electrodes were assembled by the thermal decomposition of 0.01 M H$_2$PtCl$_6$ (Sigma-Aldrich) in isopropyl alcohol (Sigma-Aldrich) and spun on FTO substrates followed by sintering at 450 °C for 30 min.

2.3 Characterization

The surface morphologies of the VKS and spin-coated TiO$_2$ thin films were evaluated by field-emission scanning electron microscopy (JEOL-JSM 6330F) and high-resolution transmission electron microscopy (JEOL-JEM 2100F). Cross-sectional specimens were prepared for TEM observations using a focused ion beam (Hitachi-FB 2100). The optical transmittance spectra of the TiO$_2$ BL coating were recorded using an UV/VIS/NIR spectrophotometer (UV-Vis-NIR JASCO) in the visible wavelength range. The incident photon-to-current conversion efficiency (IPCE) of the DSSCs was measured using a PV Measurements Inc. device (Model QEX7) with bias illumination with reference to a calibrated silicon diode. The current-voltage characteristics of the DSSCs were obtained under 1 sun illumination (AM 1.5G, 100 mW cm^{-2}) using a Newport (USA) solar simulator (300W Xe source) and a Keithley 2400 source meter (active area of 0.25 cm^2 with a shadow mask). The conductivities of the TiO$_2$ BL coatings were obtained by the two-probe method (B1500A Semiconductor Device Analyzer, Agilent technologies, Korea). The results are summarized in J-V plots.

3. Results and Discussion

3.1 Powder Analysis

Figure 2(a) and (b) show TEM micrographs of the as-received and jet-milled powders, respectively. The as-received powder has a hard agglomerated shape consisting of nano-sized primary particles, but no defects were observed in the particles. By contrast, the number of defects (indicated by the black arrows) significantly increased, and some part of the granules was separated after the jet-milling process, as observed in Fig. 2(b). However, the mean particle size was not significantly reduced (from 123 to 120 nm) during the pretreatment, as confirmed in Fig. 3(a). There was a slight change of the size distribution range. In addition, the phase was preserved as an anatase phase after jet-milling, as shown in Fig. 3(b).

3.2 Selection of the VKS Process Conditions for the DSSC Blocking Layer

Many VKS films were fabricated in order to investigate the blocking layer performance. Figure 4 shows FESEM cross-sectional micrographs of the films formed under various process conditions. At the same traverse speed, the coating thickness increased as the mass flow rate increased, which may be related to the deposition rate which is affected by the particle kinetic energy (Ref 33, 34). At the same mass flow, the film thickness decreased as the traverse speed increased because the amount of particles taking part in the deposition decreased the unit surface area as the nozzle gun speed increased. However, the transmittance tended to decrease considerably as the BL thickness increased, which deteriorates the performance of the DSSC (Ref 35). Consequently, thick VKS films (around 100 nm) were excluded from the candidates as a blocking layer, where the thinnest and thickest films among the others in Fig. 4 were selected to apply as a BL in the DSSC assembly. In this research, the thinnest (MF = 3, Ts = 5) and thickest films (MF = 5, Ts = 1) are denoted as VKS1-BL and VKS2-BL, respectively, as shown in Fig. 4.
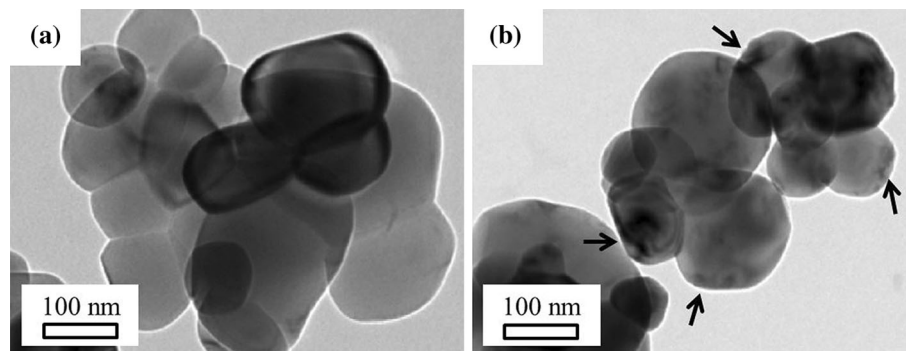

Fig. 2 TEM micrographs of the (a) as-received and (b) jet-milled (defects indicated by the black arrows) TiO$_2$ powders
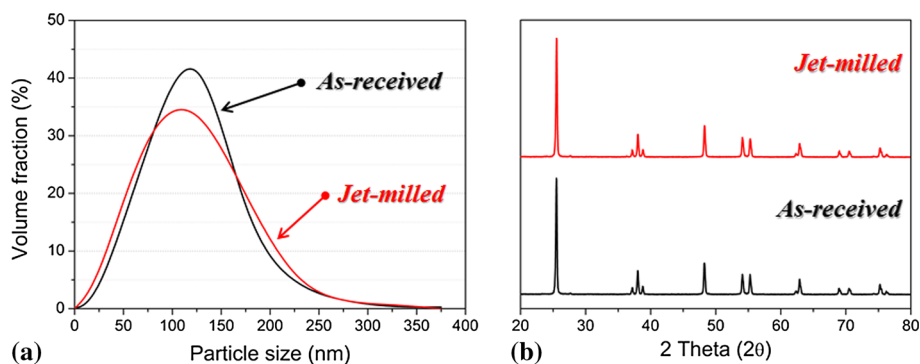
Fig. 3 (a) Particle size distributions and (b) XRD peaks of the as-received and jet-milled powders
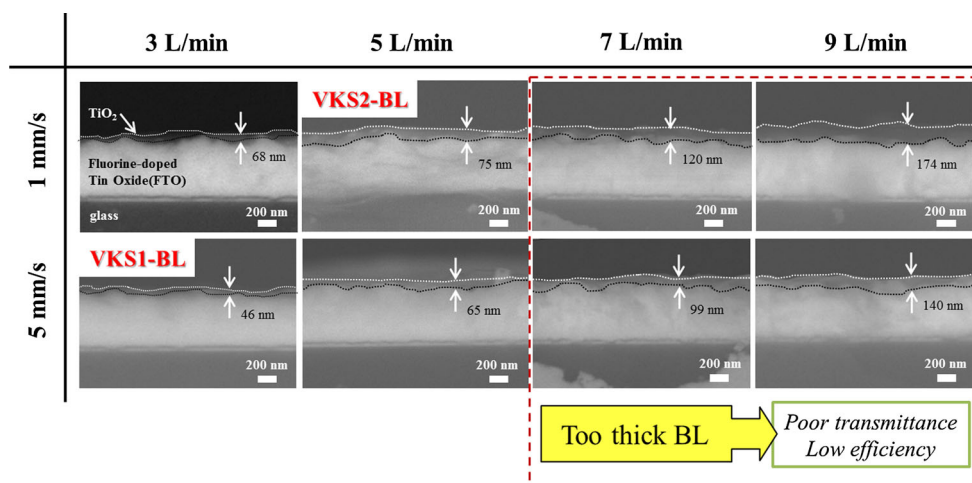

Fig. 4 Cross-sectional FESEM micrographs of various VKS films fabricated under different process conditions for the application of a blocking layer. The horizontal and vertical axes represent the mass flow rate (L/min) and traverse speed (mm/s), respectively

3.3 Microstructural Features of the Spin-Coated and Vacuum Kinetic Sprayed Films

The surface morphologies of the bare and TiO_2 film spin-coated FTO surfaces are presented in Fig. 5(a) and (b), respectively. The results clearly show that the high surface roughness of the FTO surface is covered with a TiO_2 nanocrystalline film by spin coating, as shown in Fig. 5(b). At low magnification, defects were observed on the spin-coated TiO_2 film, as seen in Fig. 5(c). The black dashed box in Fig. 5(c) was observed under high magnification, as shown in Fig. 5(d), and the section of the black dashed circle in Fig. 5(d) was magnified with a small tilt degree, as shown in Fig. 5(e), where it was confirmed that the spin-coated film was around 50 nm thick and peeled off as the surface of the FTO substrate was exposed. During the spinning process, the solution was physically ejected away from the substrate surface by centrifugal force. Thus, crystallization does not take place in the uncovered areas, which results in coating defects. These defects typically occur when the spin and coating properties are not set appropriately or when dust or nonuniformity of the surface tension on the substrate surface exists (Ref 21). It is a concern that electrons can leak to

the electrolyte through these defect centers and affect the photocurrent collection at the DSSCs.

The SEM images of VKS1 and VKS2-BL are presented in Fig. 6(a) and (b), respectively. The comparison of the crystallite nature in Fig. 5(b) and 6 clearly illustrates that the coating texture depends on the coating technique. The spin-coated BL contains an inhomogeneous spherical TiO_2 crystallite formation (bigger and smaller particles) compared to the VKS-coated BL. Meanwhile, it can be seen that the compact TiO_2 film uniformly adheres on the FTO substrate. The coating surface of the spin-coated BL looks rougher than that of the VKS-coated BL, and the roughness of VKS1-BL seems to be higher than that of VKS2-BL, as shown in Fig. 5(b), 6(a), and (b). However, since the roughness of the blocking layer, which works to prevent electron recombination through FTO and provide better connection with the TiO_2 semiconducting layer in the dye-sensitized solar cell, is generally not important, unlike other solar cells such as organic solar cells and silicon-based solar cells, the effect of the coating roughness was not considered in this study.

The VKS1 and VKS2-BL coating layers were estimated to about 46 and 76 nm, respectively, as indicated by the
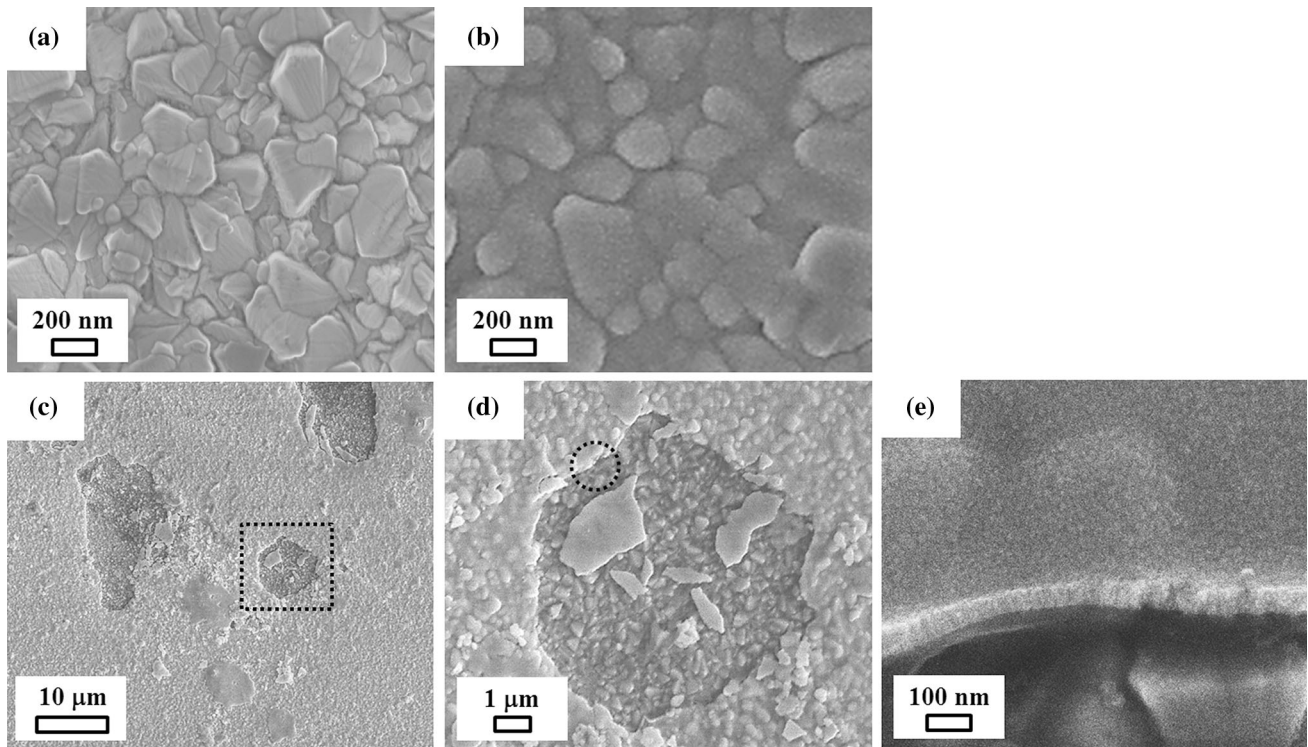
Fig. 5 FESEM images of the (a) bare FTO substrate and (b) TiO$_2$ spin-coated FTO. (c) Low-magnification SEM image of the TiO$_2$ spin-coated FTO morphology, and higher magnification images of the (d) black dashed box and (e) circle in (c) and (d), respectively
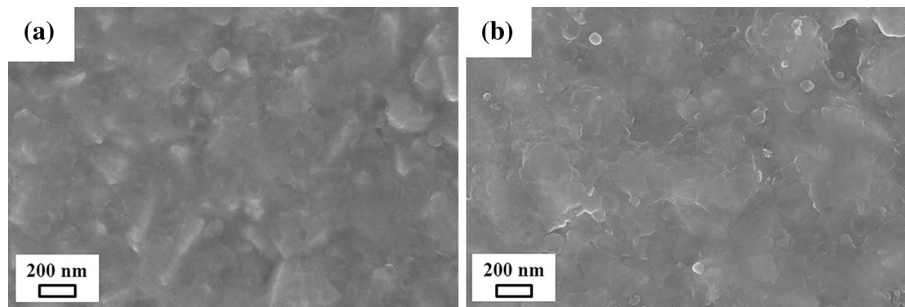

Fig. 6 FESEM surface morphologies of the VKS TiO$_2$ coatings: (a) VKS1-BL and (b) VKS2-BL

black and white dashed lines in Fig. 4. Although the VKS1-BL film was thinner, its film thickness uniformity was slightly worse than that of VKS2-BL. In addition, it can be expected that a more compact microstructure was formed in VKS2-BL in light of the tamping effect at a high particle velocity (Ref 36, 37). This compact layer is considered to be better suited to prevent contact of the electrolyte and FTO, which reduces the probability of recombination (Ref 38). Based on the above observations, it is expected that the dense coating texture in the VKS coating will be more advantageous in achieving uniform and mechanically stable coatings on high surface roughness substrates such as FTO, even without post-treatment. In other words, the compact VKS BL can decrease light scattering and provide more charge injection pathways by uniformly covering the rough FTO surface while electron

tunneling transport from FTO to the mp-TiO$_2$ layer can occur through the less-compact spin-coated BL.

The microstructure and composition of the VKS-coated TiO$_2$ films were evaluated by cross-sectional TEM images, where a typical image is presented in Fig. 7. The cross-sectional image of the VKS2-BL in Fig. 7(a) shows a distinct TiO$_2$/FTO interface where the thickness of the TiO$_2$ coating was found to be 72 nm, which corresponds to the thickness observed in the SEM image in Fig. 6(b). Furthermore, it was evident that the TiO$_2$ coating adhered well to the FTO surface such that the coating/substrate interface was quite intimate, without any cracks or pores, as confirmed in Fig. 7(b). This intimate interface is one of the typical features of a VKS coating, and it is thought that the interface was formed by a particle impact-induced deposition process in which the bonding between the
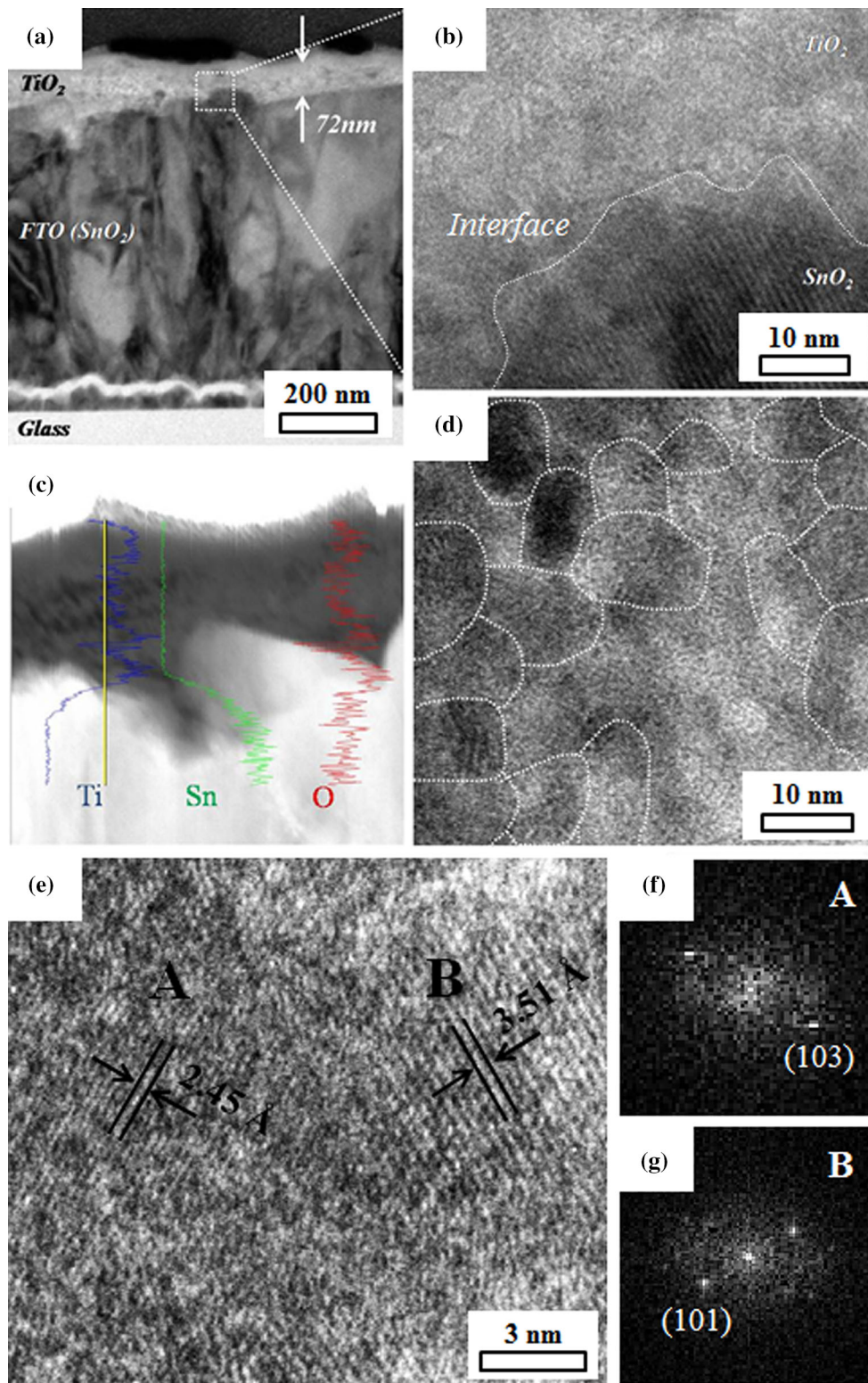
Fig. 7 (a) Cross-sectional TEM images of the VKS2-BL TiO$_2$-coated FTO and the (b) intimate coating/FTO interface shown in the white dashed boxed region in (a). Elemental analysis at the (c) TiO$_2$/FTO interface across the yellow line, (d) polycrystal coating layer (the grains are enclosed by white dashed lines), and (e) interface between two grains. FFT patterns of the (f) A and (g) B sites

coating layer and substrate becomes stronger as the particle velocity increases (Ref 33). Also, the interface between the coating layer and tin oxide was confirmed using elemental analysis, as shown in Fig. 7(c). The coating layer is comprised nano-sized grains with random orientations, as observed in Fig. 7(d). This is a typical feature of coating layers fabricated by the VKS process (Ref 25, 39). The polycrystal structure was analyzed in the high-magnification TEM images as shown in Fig. 7(e)-(g). Figure 7(e) shows the interface between the A and B grains with different lattice orientations. In both the A and B regions, the crystallites were analyzed by Fast Fourier transform (FFT) patterns, as shown in Fig. 7(f) and (g). The FFT patterns confirmed the (103) and (101) lattice planes, which correspond to the anatase TiO_2 crystallite phase with interspacings of 2.45 and 3.5 Å, respectively. Several nano-sized grains in the coating seem to be submicron-sized powders that were fragmented to nano-sized particles during the deposition process and, hence, formed compact and strong particle to particle bonds (Ref 25, 28). In the other samples, there was no difference of the microstructure in terms of the mean grain size, which was approximately 10 nm, and compact bonding. The only noted difference is the coating thickness. These findings suggest that VKS BL is effective to impart a compact BL in DSSCs.

3.4 Optical and Conductivity Analysis

The optical transmittance spectra of the different TiO_2 BL coatings are presented in Fig. 8. In Fig. 8, the spin-coated TiO_2 BL shows a high transmittance compared to the VKS-coated samples, which may be ascribed to the fact that they are less dense and compact. Comparing the VKS-coated TiO_2 electrodes, VKS1-BL results in a relatively high transmittance (~74%) compared to VKS2-BL. The decrement of the transmittance may be attributed to the thickness or crystallite texture effect. From Fig. 6, it is evident that the VKS2-BL coating is denser and thicker than VKS1-BL, and the highly compact nature of the TiO_2 BL at the VKS2-BL electrode results in reduced transmittance. Allowing for light illumination, a BL with a lower
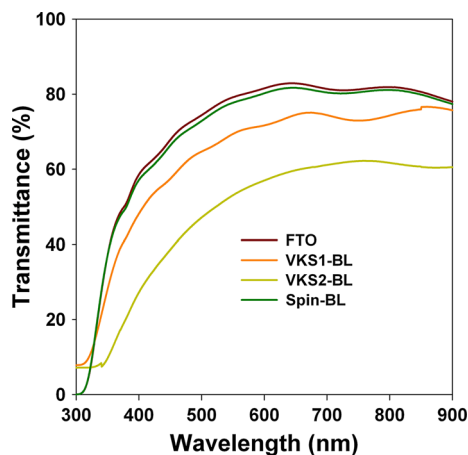
transmittance may affect the light-harvesting efficiency of DSSCs.

The conductivity of the TiO_2 BL coatings was studied by the two-probe method, and the resultant J-V plots are summarized in Fig. 9. As discussed previously, the blocking layers have different thicknesses. Therefore, the data reported in Fig. 9 represent the conductance of the films rather than the material's specific conductivity. Linear current density-voltage characteristics were observed for the spin-coated TiO_2 films, which confirmed the ohmic behavior of this sample. It has been reported that electron tunneling transport can occur with less-compact TiO_2 films. In the case of VKS-coated TiO_2, a non-linear J-V curve was obtained due to the inclusion of resistivity in the circuit, which reduced the number of tunneling electrons across the junction. The more compact VKS2-BL coating resulted in high-resistivity films which shifted the J-V curve toward a high voltage, suggesting that it required more operating potential to move electrons across the junction. Based on this result, the VKS1-BL coating is thought to be more effective in DSSCs than the less-compact Spin BL or the highly thick and compact VKS2-BL.

3.5 Photovoltaic Performance

The photovoltaic performances of the DSSCs composed of different blocking layers which were studied, and the resultant J-V plots are presented in Fig. 10. The photovoltaic parameters were estimated using the results shown in Fig. 10 and are listed in Table 2. As shown in Table 2, the DSSCs without a BL showed a η (photoconversion efficiency, PCE) of 3.3% with a V_{oc} (open-circuit voltage) of 0.64 V, a J_{sc} (short-circuit current density) of 7.9 mA cm^{-2}, and a F.F. (fill factor) of 67.7%. After applying the VKS-coated BL in DSSCs, the PCE markedly improved to η = 5.6% with a V_{oc} of 0.76 V, a J_{sc} of 10.3 mA cm^{-2}, and a F.F. of 72.4%. Approximately 69% enhancement of the PCE is due to the blocking of electron leakage from the FTO surface to the electrolyte through uncovered TiO_2 sites. In the case of the VKS2-BL
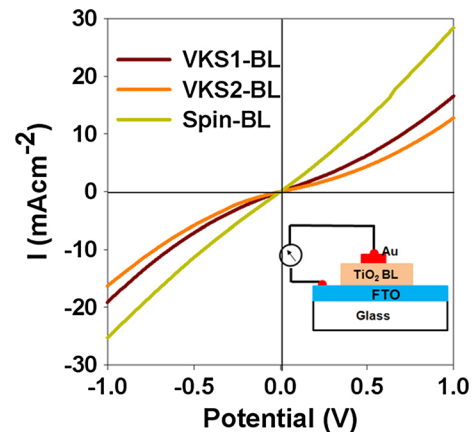

Fig. 8 Optical transmittance spectra of the bare and TiO_2 BL-coated FTO substrates

Fig. 9 Current-voltage characteristics of the compact TiO_2 blocking layer between two electrodes. The inset shows a schematic of the metal/semiconductor/metal configuration for the two-probe measurements
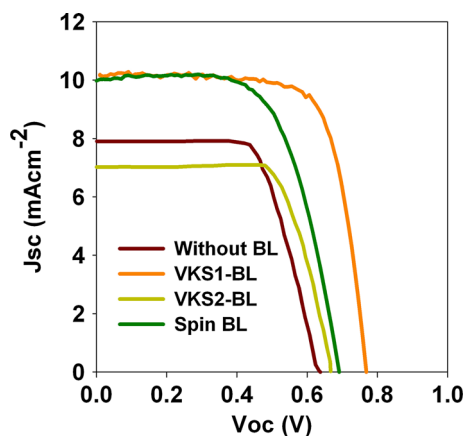
Fig. 10 J-V plots of the DSSCs with different TiO_2 blocking layers

Fig. 11 IPCE spectra of the DSSCs with different TiO_2 blocking layers

Table 2 Photovoltaic parameters

Blocking layers	Voc, V	Jsc, mA cm^{-2}	F.F., %	η, %
Without BL	0.64	7.9	67.7	3.3
VKS1-BL	0.76	10.3	72.4	5.6
VKS2-BL	0.67	7.0	72.4	3.4
Spin BL	0.69	9.9	65.0	4.4

layer-based DSSCs, the PCE was drastically reduced to $\eta = 3.4\%$ with a severe loss of $V_{oc} = 0.67$ V and $J_{sc} = 7.0$ mA cm^{-2}. The decrease of the J_{sc} value is due to the highly resistant nature of the thick BL layer in between the FTO and mp TiO_2 coating interface, which blocks the forward electron transport from the mp TiO_2 layer to the charge collectors (Ref 40). In addition, the blockage of electrons at the FTO/mp TiO_2 interface results in high charge accumulation at the Fermi level of the mp TiO_2 layer, leading to recombination through the redox shuttle at the electrolyte, which reduces the V_{oc} of the device. The high PCE performance of the VKS1-BL-coated DSSCs is due to effective blockage of backward electron flow from the FTO surface to the electrolyte as well as efficient forward charge injection from the mp TiO_2 layer to the FTO charge collector layers. Because of managing both the forward charge transport and retarding the backward electron flow at FTO/mp TiO_2 interfaces, the VKS1-BL-coated device showed a higher performance than the spin-coated BL layer devices. In consideration of the similar coating thicknesses of VKS1-BL and the spin-coated BL, as shown in Fig. 5(e) and 6(c), it can be inferred that the difference of the DSSC performance was caused by the film condition. That is, the VKS film is very dense and uniform, which more effectively assumes the role of a blocking layer than the partially peeled off and non-uniform spin-coated BL as shown in Fig. 5(c) and (d). As a result, the high tunneling conductance through the less-compact spin-coated TiO_2 films allows tunneling recombination of backward electrons from the FTO surface. This affects the V_{oc} of the device and thus, lowers the device performance.
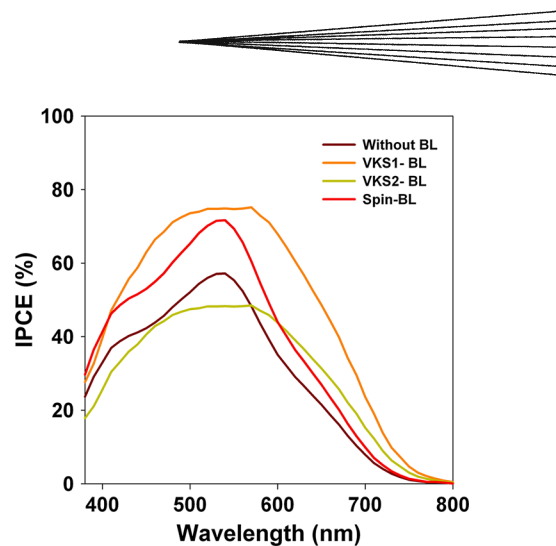
The blocking effect of the different TiO_2 coatings on the charge collection was further studied by obtaining IPCE spectra, as shown in Fig. 11. The IPCE is defined as the ratio of the number of electrons in the external circuit produced by an incident photon at a given wavelength (Ref 13). As confirmed in Fig. 10, the open-circuit voltage of VKS1 is higher than that obtained without a BL or spin-coated BL, indicating that VKS1 can block electron leakage from FTO to the electrolyte better than the others because the conditions of the cells including the electron transport layer, dye, and electrolyte are not different in the cells. Furthermore, the possibilities of forward charge injection in the VKS1-BL and spin BL-based devices are the result of their high IPCE values of approximately 75 and 70%, respectively, as confirmed in Fig. 11. This indicates that the BL in the DSSCs effectively blocks the backward flow of electrons from the FTO surface to the electrolyte and more injected electrons flow to the circuit without recombination in the DSSC with the VKS1-BL than in the Spin BL. The absence of a BL in the DSSCs resulted in severe charge recombination at the FTO/mp TiO_2 interface and reduced the charge collection to result in a low IPCE of nearly 52% of the value of the other samples. This suggests that the BL-assisted DSSCs markedly promote the PCE of DSSCs. Therefore, highly dense crystallite TiO_2 with an apparent electronic conductivity achieved by the VKS technique was shown to be beneficial in DSSCs.

4. Conclusions

In this study, a uniform and dense blocking layer (BL) was fabricated on a FTO substrate by the vacuum kinetic spray coating (VKS) process to improve the photoconversion efficiency (PCE) of dye-sensitized solar cells (DSSCs). Various BLs with different thicknesses were generated by controlling the VKS mass flow rate and traverse speed, and were compared with Spin BLs in terms of the microstructure and photovoltaic characteristics. In

the case of the VKS BL, the fragmented particles were densely bonded in the coating layer, and the coating/substrate interface was well formed, without cracks or pores. This compact and uniform coating texture in the VKS BL was more effective in improving the performance of the DSSCs because of their uniform and mechanically stable coatings on high surface roughness substrates such as FTO. When compared to the DSSC without a BL, the PCE of the DSSC with the VKS1-BL with a thickness of 46 nm increased from 3.3 to 5.6%. The enhancement of the PCE by about 69% is due to the blocking of electron leakage from the FTO surface to the electrolyte. This value was also higher than that of the DSSC with a Spin BL because of the management of the forward charge injection and retardation of the backward electron flow at the FTO/mp-TiO$_2$ interface. Therefore, VKS is an outstanding method for preparing a BL to improve the performance of DSSCs.

Acknowledgment

References

1. B. Oregan and M. Gratzel, A Low-Cost, High-Efficiency Solar-Cell Based on Dye-Sensitized Colloidal TiO$_2$ Films, *Nature*, 1991, **353**, p 737-740

2. A. Hagfeldt, G. Boschloo, L.C. Sun, L. Kloo, and H. Pettersson, Dye-Sensitized Solar Cells, *Chem. Rev.*, 2010, **110**, p 6595-6663

3. M. Law, L.E. Greene, J.C. Johnson, R. Saykally, and P.D. Yang, Nanowire Dye-Sensitized Solar Cells, *Nat. Mater.*, 2005, **4**, p 455-459

4. A. Nattestad, A.J. Mozer, M.K.R. Fischer, Y.B. Cheng, A. Mishra, P. Bauerle, and U. Bach, Highly Efficient Photocathodes for Dye-Sensitized Tandem Solar Cells, *Nat. Mater.*, 2010, **9**, p 31-35

5. J.H. Yum, E. Baranoff, F. Kessler, T. Moehl, S. Ahmad, T. Bessho, A. Marchioro, E. Ghadiri, J.E. Moser, C.Y. Yi, M.K. Nazeeruddin, and M. Gratzel, A Cobalt Complex Redox Shuttle for Dye-Sensitized Solar Cells with High Open-Circuit Potentials, *Nat. Commun.*, 2012, **3**, p 1-8

6. J.R. Jennings, Y. Liu, Q. Wang, S.M. Zakeeruddin, and M. Gratzel, The Influence of Dye Structure on Charge Recombination in Dye-Sensitized Solar Cells, *Phys. Chem. Chem. Phys.*, 2011, **13**, p 6637-6648

7. M.S. Kang, J.H. Kim, J. Won, and Y.S. Kang, Oligomer Approaches for Solid-State Dye-Sensitized Solar Cells Employing Polymer Electrolytes, *J. Phys. Chem. C*, 2007, **111**, p 5222-5228

8. P. Sudhagar, S. Nagarajan, Y.G. Lee, D. Song, T. Son, W. Cho, M. Heo, K. Lee, J. Won, and Y.S. Kang, Synergistic Catalytic Effect of a Composite (CoS/PEDOT:PSS) Counter Electrode on Triiodide Reduction in Dye-Sensitized Solar Cells, *ACS Appl. Mater. Interfaces.*, 2011, **3**, p 1838-1843

9. Y.G. Lee, S. Park, W. Cho, T. Son, P. Sudhagar, J.H. Jung, S. Wooh, K. Char, and Y.S. Kang, Effective Passivation of Nanostructured TiO$_2$ Interfaces with PEG-Based Oligomeric Coadsorbents to Improve the Performance of Dye-Sensitized Solar Cells, *J. Phys. Chem. C*, 2012, **116**, p 6770-6777

10. A. Yella, H.W. Lee, H.N. Tsao, C.Y. Yi, and A.K. Chandiran, Porphyrin-Sensitized Solar Cells with Cobalt (II/III)-Based Redox Electrolyte Exceed 12 Percent Efficiency, *Science*, 2011, **334**, p 629-634

11. U. Bach, D. Lupo, P. Comte, J.E. Moser, F. Weissortel, J. Salbeck, H. Spreitzer, and M. Gratzel, Solid-State Dye-Sensitized Mesoporous TiO$_2$ Solar Cells with High Photon-to-Electron Conversion Efficiencies, *Nature*, 1998, **395**, p 583-585

12. P. Wang, S.M. Zakeeruddin, J.E. Moser, M.K. Nazeeruddin, T. Sekiguchi, and M. Gratzel, A Stable Quasi-Solid-State Dye-Sensitized Solar Cell with an Amphiphilic Ruthenium Sensitizer and Polymer Gel Electrolyte, *Nat. Mater.*, 2003, **2**, p 498

13. H. Yu, S. Zhang, H. Zhao, G. Will, and P. Liu, An Efficient and Low-Cost TiO$_2$ Compact Layer for Performance Improvement of Dye-Sensitized Solar Cells, *Electrochem. Acta*, 2009, **54**, p 1319-1324

14. H.-J. Kim, J.-D. Jeon, D.Y. Kim, J.-J. Lee, and S.-Y. Kwak, Improved Performance of Dye-Sensitized Solar Cells with Compact TiO$_2$ Blocking Layer Prepared Using Low-Temperature Reactive ICP-Assisted DC Magnetron Sputtering, *J. Ind. Eng. Chem.*, 2012, **18**, p 1807-1812

15. D. Qian, Y. Li, Q. Zhang, G. Shi, and H. Wang, Anatase TiO$_2$ Sols Derived from Peroxotitanium Acid and to Form Transparent TiO$_2$ Compact Film for Dye-Sensitized Solar Cells, *J. Alloys Compd.*, 2011, **509**, p 10121-10126

16. S. Lee, D.H. Kim, J.Y. Kim, H.S. Jung, H. Shin, and K.S. Hong, Improved Spectral Response of Sensitized Photoelectrodes with the Optical Modulation Layer, *Electrochem. Commun.*, 2012, **15**, p 29-33

17. B. Peng, G. Jungmann, C. Jäger, D. Haarer, H.-W. Schmidt, and M. Thelakkat, Systematic Investigation of the Role of Compact TiO$_2$ Layer in Solid State Dye-Sensitized TiO$_2$ Solar Cells, *Coord. Chem. Rev.*, 2004, **248**, p 1479-1489

18. S.M. Waita, B.O. Aduda, J.M. Mwabora, G.A. Niklasson, C.G. Granqvist, and G. Boschloo, Electrochemical Characterization of TiO$_2$ Blocking Layers Prepared by Reactive DC Magnetron Sputtering, *J. Electroanal. Chem.*, 2009, **637**, p 79-83

19. J.G. Lee, J.H. Cheon, H.S. Yang, D.K. Lee, and J.H. Kim, Enhancement of Photovoltaic Performance in Dye-Sensitized Solar Cells with the Spin-Coated TiO$_2$ Blocking Layer, *J. Nanosci. Nanotechnol.*, 2012, **12**, p 6026-6030

20. T.Y. Cho, S.G. Yoon, S.S. Sekhon, M.G. Kang, and C.H. Han, The Effect of a Sol-Gel Formed TiO$_2$ Blocking Layer on the Efficiency of Dye-Sensitized Solar Cells, *B. Korean Chem. Soc.*, 2011, **32**, p 3629-3633

21. J.F. Taylor, *Spin coating: An Overview*, Sony Chemicals Corp. of America, Mt. Pleasant, 2001

22. H. Kozuka, S. Takenaka, and S. Kimura, Nanoscale Radiative Striations of Sol-Gel-Derived Spin-Coating Films, *Scr. Mater.*, 2001, **44**, p 1807-1811

23. K. Chen, Z. Lü, N. Ai, X. Huang, Y. Zhang, X. Ge, X. Xin, X. Chen, and W. Su, Fabrication and Performance of Anode-Supported YSZ Films by Slurry Spin Coating, *Solid State Ion.*, 2007, **177**, p 3455-3460

24. J.-A. Jeong and H.-K. Kim, Thickness Effect of RF Sputtered TiO$_2$ Passivating Layer on the Performance of Dye-Sensitized Solar Cells, *Sol. Energ. Mater. Sol. C*, 2011, **95**, p 344-348

25. J. Akedo, Room Temperature Impact Consolidation (RTIC) of Fine Ceramic Powder by Aerosol Deposition Method and Applications to Microdevices, *J. Therm. Spray Technol.*, 2008, **17**, p 181-198

26. J. Akedo, Aerosol Deposition of Ceramic Thick Films at Room Temperature: Densification Mechanism of Ceramic Layers, *J. Am. Ceram. Soc.*, 2006, **89**, p 1834-1839

27. D. Popovici and J. Akedo, Control of powder quality as a method of improving the dielectric properties of (Ba$_{0.6}$,Sr$_{0.4}$)TiO$_3$ thick films fabricated by aerosol deposition method, *Jpn. J. Appl. Phys.*, 2010, 49, p.09MA13-09MA13-5

28. S.M. Nam, N. Mori, H. Kakemoto, S. Wada, J. Akedo, and T. Tsurumi, Alumina Thick Films as Integral Substrates Using Aerosol Deposition Method, *Jpn. J. Appl. Phys.*, 2004, **43**, p 5414-5418

29. F. Cao, H. Park, G. Bae, J. Heo, and C. Lee, Microstructure Evolution of Titanium Nitride Film During Vacuum Kinetic Spraying, *J. Am. Ceram. Soc.*, 2013, **96**(1), p 40-43
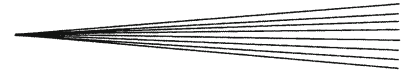
30. D.M. Chun and S.H. Ahn, Deposition Mechanism of Dry Sprayed Ceramic Particles at Room Temperature Using a Nano-particle Deposition System, *Acta Mater.*, 2011, **59**, p 2693-2703

31. D.-W. Lee, H.-J. Kim, Y.-H. Kim, Y.-H. Yun, and S.-M. Nam, Growth Process of α-Al₂O₃ Ceramic Films on Metal Substrates Fabricated at Room Temperature by Aerosol Deposition, *J. Am. Ceram. Soc.*, 2011, **94**(9), p 3131-3138

32. A. Iwata and J. Akedo, Hexagonal to Cubic Crystal Structure Transformation During Aerosol Deposition of Aluminum Nitride, *J. Crystal. Growth*, 2005, **275**, p e1269-e1273

33. F. Cao, H. Park, J. Heo, J. Kwon, and C. Lee, Effect of Process Gas Flow on the Coating Microstructure and Mechanical Properties of Vacuum Kinetic-Sprayed TiN Layers, *J. Therm. Spray Technol.*, 2013, **22**(7), p 1109-1119

34. K. Naoe, M. Nishiki, and A. Yumoto, Relationship Between Impact Velocity of Al₂O₃ Particles and Deposition Efficiency in Aerosol Deposition Method, *J. Therm. Spray Technol.*, 2013, **22**(8), p 1267-1274

35. S.W. Lee, J.H. Noh, H.S. Han, D.K. Yim, D.H. Kim, J.-K. Lee, J.Y. Kim, H.S. Jung, and K.S. Hong, Nb-Doped TiO₂: A New Compact Layer Material for TiO₂ Dye-Sensitized Solar Cells, *J. Phys. Chem. C*, 2009, **113**, p 6878-6882

36. S.-Q. Fan, G.-J. Yang, C.-J. Li, G.-J. Liu, C.-X. Li, and L.-Z. Zhang, Characterization of Microstructure of Nano-TiO₂ Coating Deposited by Vacuum Cold Spraying, *J. Therm. Spray Technol.*, 2006, **15**(4), p 513-517

37. C.-J. Li and W.-Y. Li, Deposition Characteristics of Titanium Coating in Cold Spraying, *Surf. Coat. Technol.*, 2003, **167**, p 278-283

38. B. Bills, M. Shanmugam, and M.F. Baroughi, Effects of Atomic Layer Deposited HfO₂ Compact Layer on the Performance of Dye-Sensitized Solar Cells, *Thin Solid Films*, 2011, **519**, p 7803-7808

39. H. Park, H. Heo, F. Cao, J. Kwon, K. Kang, G. Bae, and C. Lee, Deposition Behavior and Microstructural Features of Vacuum Kinetic Sprayed Aluminum Nitride, *J. Therm. Spray Technol.*, 2013, **22**(6), p 882-891

40. B.J. Choi, D.S. Jeong, and S.K. Kim, Resistive Switching Mechanism of TiO₂ Thin Films Grown by Atomic-Layer Deposition, *J. Appl. Phys.*, 2005, **98**, p 033715-033724